Antiviral Research 103 (2014) 60–70

Contents lists available at ScienceDirect

Antiviral Research

journal homepage: www.elsevier.com/locate/antiviral

The competitive binding between inhibitors and substrates of HCV NS3/4A protease: A general mechanism of drug resistance

Yan Guan [a], Huiyong Sun [a], Youyong Li [a], Peichen Pan [a], Dan Li [b], Tingjun Hou [a,b,*]

[a] Institute of Functional Nano & Soft Materials (FUNSOM) and Collaborative Innovation Center of Suzhou Nano Science and Technology, Soochow University, Suzhou, Jiangsu 215123, China
[b] College of Pharmaceutical Sciences, Zhejiang University, Hangzhou, Zhejiang 310058, China

ARTICLE INFO

Article history:
Received 15 October 2013
Revised 5 January 2014
Accepted 13 January 2014
Available online 23 January 2014

Keywords:
HCV
Drug resistance
Molecular dynamics
MM/GBSA
Substrate envelope hypothesis

ABSTRACT

Hepatitis C virus (HCV) infection is a serious public health problem throughout the world. Great success has been achieved in developing inhibitors targeting the HCV NS3/4A protease over the past decade, but the rapid emergence of drug resistant mutations greatly compromises the efficacy of antiviral drugs or drug candidates. According to the substrate envelope hypothesis (Romano et al., 2010), severe drug resistant mutations would always occur where the inhibitors protrude from the substrate envelope, defined as a consensus volume occupied by the viral substrates in the active site of the NS3/4A protease. However, the substrate envelope hypothesis just qualitatively assesses the impact of mutations to a specific inhibitor, but no quantitative data is obtained. To remedy the weakness, the dynamic binding patterns of HCV NS3/4A protease inhibitors or substrates were investigated by molecular dynamics (MD) simulations and continuum solvation binding affinity predictions in this study. By comparing the quantitative binding profiles between the substrates and inhibitors, derived from the free energy decomposition analysis, we observed most residues involved in drug resistance form stronger interactions with the inhibitors than with the substrates, which is roughly coincident with the substrate envelope hypothesis and supports the general mechanism of drug resistance: the critical resistant mutations impair more to the binding of inhibitors than that of substrates. Furthermore, our predictions illustrate that the natural substrates of NS3/4A form balanced interactions with the strands 135–139 and 154–160 whereas the inhibitors cannot. Therefore, to overcome drug resistance, it may be necessary to restore the interaction balance between the two strands and the drug candidates. To our disappointment, the underlying resistant mechanisms of some mutations could not be well captured by just comparing the binding profiles of inhibitors and substrates, and more studies should be proceeded to propose a general drug resistance mechanism.

1. Introductions

Hepatitis C virus infection is a main cause of chronic liver disease and liver transplantation. It is estimated that more than 150 million people are chronically infected with HCV worldwide and nearly 35,000 people daily die from HCV persistent infection and its sequelae. The previous standard of care (SOC) comprising the pegylated interferon-α (IFN-α) and ribavirin (RBV) showed sustained virological response (SVR) of only about 40–50% in patients infected with genotype-1 (GT-1) HCV, whereas the SVR rates of approximately 75% and 60% were achieved in patients infected with HCV GT-2 or GT-3 and GT-4 (Almasio et al., 2007; Fried et al., 2002; Jamall et al., 2008). To improve the efficacy, the current SOC comprising the pegylated interferon-α and RBV plus direct-acting antiviral agents (DAA), that are NS3/4A protease inhibitors either telaprevir or boceprevir. Extensive studies have confirmed improved SVR rates up to 79–80% in GT-1 infected patients due to the addition of a protease inhibitor (Bacon et al., 2011; McHutchison et al., 2010).

The HCV genome consists of 9600 nucleotides encoding a polyprotein precursor for which later cleaved into at least ten viral proteins, including four structural proteins (core, E1, E2 and P7) and six nonstructural proteins (NS2, NS3, NS4A, NS4B, NS5A and NS5B). The HCV NS3/4A protease, formed by the non-covalent association of the NS3 protease and NS4A, is an attractive target for HCV antiviral therapy. It participates in the production of mature viral proteins by catalyzing the precursor cleavage at junctions of NS3–NS4A, NS4A–NS4B, NS4B–NS5A and NS5A–NS5B (Manabe et al., 1994; Moradpour et al., 2007). In recent years, direct-acting antiviral therapy (DAA) targeting the NS3/4A protease

* Corresponding author at: Institute of Functional Nano & Soft Materials (FUNSOM) and Collaborative Innovation Center of Suzhou Nano Science and Technology, Soochow University, Suzhou, Jiangsu 215123, China.
E-mail addresses: tingjunhou@hotmail.com, tingjunhou@zju.edu.cn (T. Hou).

0166-3542/$ - see front matter © 2014 Elsevier B.V. All rights reserved.
http://dx.doi.org/10.1016/j.antiviral.2014.01.010

is basking in a great boom. Telaprevir, boceprevir and simeprevir (TMC435) have been successively approved by FDA for the therapy of GT-1 HCV patients (McHutchison et al., 2009). Meanwhile, other promising NS3/4A inhibitors, such as ACH1625, ITMN191, MK7009, SCH900518, MK5172, and BI201335, are also under clinical trials (Fig. 1) (Halfon and Locarnini, 2011; Welsch et al., 2012a). Despite the great success, the rapid emergence of drug-resistant mutations significantly compromises the therapeutic efficacy. Almost all NS3/4A inhibitors were found to induce resistance variations in *in vitro* replicon experiments and/or in clinical trials (Table S1 in Supporting Materials) (Forestier et al., 2011; Perni et al., 2006; Tong et al., 2010; Wohnsland et al., 2007). The resistance levels differ in mutated sites and inhibitors, and among them, the mutations at Arg155, Ala156 and Asp168 are common in patients with GT-1 (Lenz et al., 2010; Sarrazin and Zeuzem, 2010). Some variations appeared under the selective pressure of drugs or other factors whereas the others such as R155K are pre-existent before the treatment (Colson et al., 2008; Rong et al., 2010). NS3/4A mutations were reported to impair the fitness of HCV replicons (Shimakami et al., 2011). But the drug resistant mechanisms for many mutations have not been fully understood, so there is a crucial need to explore the drug resistant mechanism, which may help to develop drug candidates effective not only to the wild-type (WT) NS3/4A protease but also to its variants.

In recent years, molecular modeling techniques provide a new way to elucidate the molecular mechanisms of the mutation-induced drug resistance for different drug targets (Hou et al., 2008a, 2009a; Hou and Yu, 2007; Karthick et al., 2012; Li et al., 2011, 2012; Liu et al., 2010; Ozen et al., 2011; Sun and Ji, 2012; Xue et al., 2012a,b,c; Zhang et al., 2010). For example, Wang et al. and Hou et al. compared the interaction profiles of the FDA-approved drugs with the natural substrates of the HIV-1 protease by using MD simulations and free energy calculations and observed that if a residue is not conserved and interacts more favorably with a drug than with the substrates, the mutation of this residue may cause resistance to the drug (Hou et al., 2008a; Wang and Kollman, 2001). Pan et al. and Xue et al. predicted the change of the binding free energies between the WT complex of TMC435

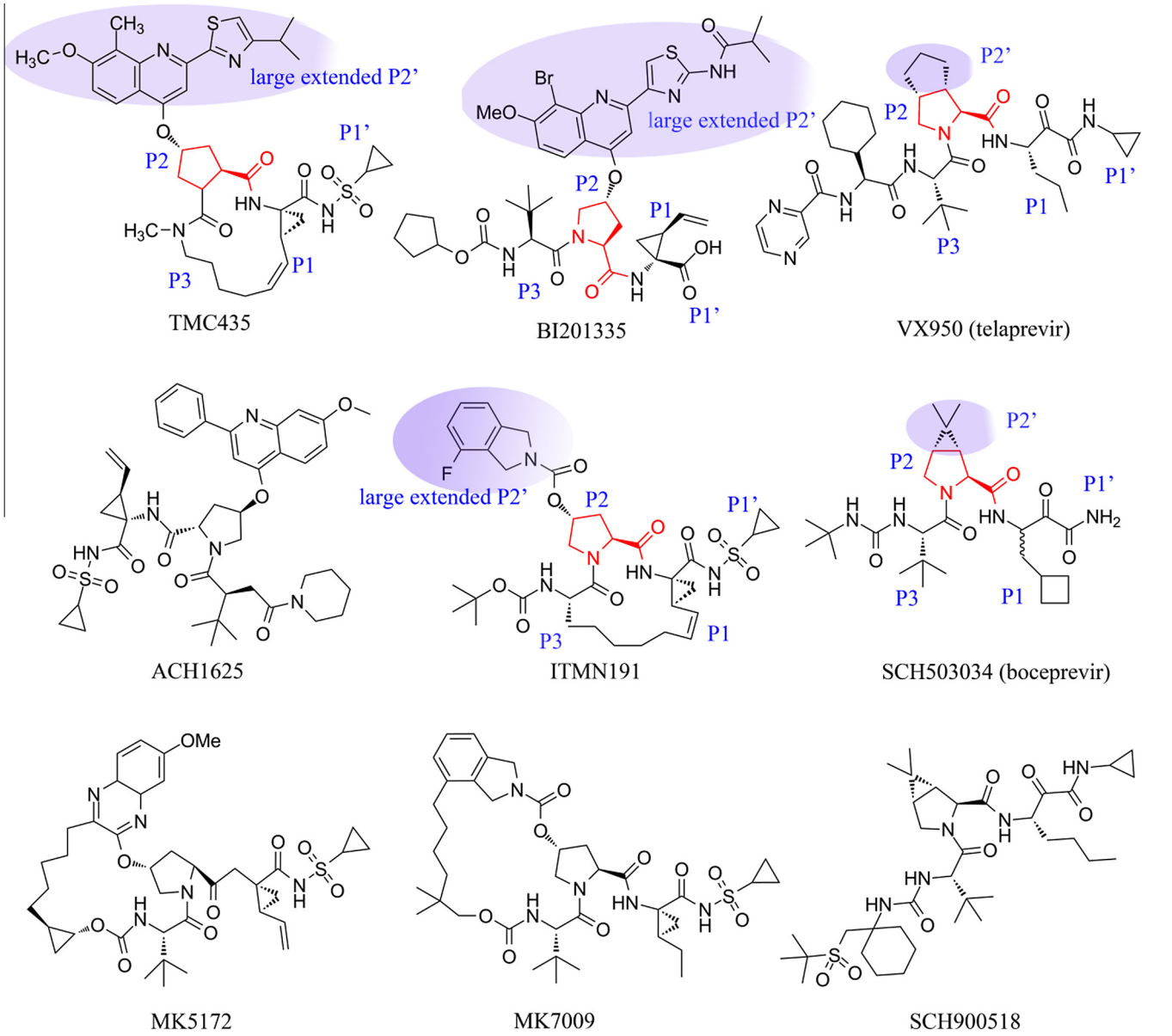

Fig. 1. Structures of the representative inhibitors of NS3/4A. The skeletons are marked by P1–P3 and P1′–P2′. Specially, P2 is marked in red and the large extended P2′ is covered with purple shadow. (For interpretation of the references to color in this figure legend, the reader is referred to the web version of this article.)

or ITMN191 and the R155K, A156V or D168A mutant (Pan et al., 2012; Xue et al., 2012a), and Welsch et al. combined MD simulations with the residue-interaction network analysis to explore the ketoamide resistance to the mutations of Val55 (Welsch et al., 2012b). However, their studies only partially illustrate the drug resistance profile to a specific inhibitor, and no study has been reported to systematically compare the binding profiles of the substrates and inhibitors of the HCV NS3/4A protease by using rigorous theoretical approaches. Therefore, in this study, the MD simulations and Molecular Mechanics/Generalized Born Solvent Area (MM/GBSA) approach were utilized to elucidate the dynamic binding patterns of three NS3/4A natural substrates (4A4B, 4B5A, and 5A5B) and five inhibitors, including boceprevir (SCH503034), telaprevir (VX950), ITMN19, TMC435 and BI201335 clinically used or under clinical trials. According to the protein–ligand interaction spectra, the studied substrates and inhibitors are structurally different, but they share similar conserved binding patterns with (1) the catalytic triad region, (2) the cross-shaped strand 135–139 and (3) the twisted strand 154–160. In addition, critical resistant mutations form stronger interactions with the inhibitors than substrates, which is consistent with the substrate envelope hypothesis. Furthermore, the substrates could form balanced interactions with the strands 135–139 and 154–160, and an inhibitor that possibly confers resistance, however, might lost the balanced interactions with them.

2. Material and methods

2.1. Preparation of structures

The crystallographic structures of the HCV GT-1 NS3/4A protease in complex with three natural substrates (4A4B, 4B5A, and 5A5B) or five inhibitors (VX950, SCH503034, ITMN191, BI201335 and TMC435) (Lemke et al., 2011; Malcolm et al., 2006; Romano et al., 2010, 2012) were retrieved from the Protein Data Bank and used as the starting structures for the MD simulations (PDB entries are listed in Table S2 in Supporting Materials). A natural peptide substrate of NS3/4A with seven residues on the N-terminus and four on the C-terminus is represented as NH2–P7–P6–P5–P4–P3–P2–P1–P1′–P2′–P3′–P4′–OH, and the corresponding binding pockets of NS3/4A are defined as S1–S7 and S1′–S4′. The studied substrates are composed of the P1–P7 segments (Table S3 in Supporting materials), and the studied inhibitors have the P4–P2′ segments (Fig. 1). The sequences of the studied substrates are listed in Table S3 in Supporting Materials and the involved inhibitors are plotted in Fig. 1.

Each inhibitor was optimized and the electrostatic potential was calculated at the HF/6-31G* level using the Gaussian09 program (Frisch et al., 2009), and the atomic partial charges were obtained by a restraint electrostatic potential fit (RESP) method (Bayly et al., 1993). The partial charges and force field parameters of each inhibitor were generated by the *antechamber* program in AMBER11 (Case et al., 2005). The zinc ion was retained for maintaining the stabilization of the systems. The *ff99SB* force field and general amber force field (*gaff*) were employed for the proteins and substrates/inhibitors, respectively (Hornak et al., 2006; Wang et al., 2004). To neutralize the systems, the counterions of Cl^- or Na^+ were added. Each system was solvated explicitly into a rectangular TIP3P (Jorgensen et al., 1983) water box that is extended 10 Å away from any solute atom.

2.2. Molecular minimization and MD simulations

Each system was first subjected to a four-stage minimization procedure by using the *sander* program in AMBER11 (Case et al., 2005). In the first stage, only the hydrogen atoms were relaxed by 1000 cycles (500 cycles of steepest descent and 500 cycles of conjugate gradient) of minimization with all heavy atoms constrained (5 kcal/mol/Å^2); next, the solvent molecules were relaxed by 1000 cycles (500 cycles of steepest descent and 500 cycles of conjugate gradient) of minimization and the other atoms were constrained (5 kcal/mol/Å^2); then, the whole system was relaxed by 1000 cycles of minimization (500 cycles of steepest descent and 500 cycles of conjugate gradient) with only the backbone atoms of the protein constrained (5 kcal/mol/Å^2); finally, all the atoms were relaxed by 5000 cycles (1000 cycles of steepest descent and 4000 cycles of conjugate gradient) of minimization without any constrain.

In the MD simulations, each system was gradually heated from 10 to 300 K over a period of 50 ps. Then, 10 ns NPT MD simulations with a target temperature of 300 K and a target pressure of 1 bar were performed. The particle-mesh Ewald (PME) algorithm was used to calculate the full electrostatic energy of a periodic box (Darden et al., 1993). The bonds involving hydrogens were constrained by the SHAKE algorithm (Ryckaert et al., 1977). A time step of 2 fs was employed in the Leapfrog integrator. Coordinates were written every 10 ps (a total of 1000 frames for each system). All the simulations were accomplished by using the *sander* program in AMBER11 (Case et al., 2005).

2.3. MM/GBSA free energy calculations

The MM/GBSA method was employed to calculate the binding free energy (ΔG_{bind}) of an inhibitor or a substrate according to the equations shown below: (Hou et al., 2011a,b, 2002; Kollman et al., 2000; Wang et al., 2006; Xu et al., 2013; Yang et al., 2011a, 2011b, 2012)

$$\Delta G_{bind} = G_{com} - (G_{rec} + G_{lig}) \quad (1)$$

$$\Delta G_{bind} = \Delta H - T\Delta S \approx \Delta E_{MM} + \Delta G_{sol} - T\Delta S \quad (2)$$

$$\Delta E_{MM} = \Delta E_{int} + \Delta E_{elec} + \Delta E_{vdw} \quad (3)$$

$$\Delta G_{sol} = \Delta G_{GB} + \Delta G_{SA} \quad (4)$$

$$\Delta_{SA} = \gamma \Delta A + b \quad (5)$$

The binding free energy (ΔE_{bind}) consists of several terms, including the gas-phase enthalpy (ΔE_{MM}), which is a sum of the internal energy (ΔE_{int}), the electrostatic interaction (ΔE_{elec}) and the van der Waals interaction (ΔE_{vd}), the solvation free energy (ΔG_{solv}) that is separated into a polar part (ΔG_{GB}) and a non-polar part (ΔG_{SA}), and the conformational entropy ($-T\Delta S$). Here, by using a single trajectory strategy, ΔE_{int} is canceled between ligand, receptor, and complex (Hou and Yu, 2007; Wang et al., 2006). The ΔG_{GB} term was calculated by using a modified GB model with the parameters developed by Onufriev et al. (referred as *igb* = 2 in AMBER) (Onufriev et al., 2004). The interior and exterior dielectric constants were set to 1 and 80, respectively. The non-polar contribution of desolvation (ΔG_{SA}) was determined based on the solvent accessible surface area (SASA) derived from the LCPO algorithm: $\Delta G_{SA} = 0.0072 \times \Delta SASA$ (Weiser et al., 1999). A total of 1000 frames evenly extracted from the 10 ns production trajectories were applied for the enthalpy calculations.

Normal mode analysis (NMA) was employed to estimate the conformational entropy ($-T\Delta S$) (Brooks and Karplus, 1983) and the distance-dependent dielectric of $4r_{ij}$ (r_{ij} is the distance between two atoms) was used for the minimization of the systems. Due to the expensive computational demand, only 20 snapshots evenly extracted from the production trajectories (10 ns) were adopted.

2.4. MM/GBSA free energy decomposition

To identify the essential binding residues of NS3/4A, the total binding free energy was further decomposed into residue-ligand pairs through the MM/GBSA decomposition scheme supported by *MMPBSA.py* in Ambertools1.5 (Hou et al., 2008b, 2009b, 2012; Miller III et al., 2012). The energy components, including ΔGelec, ΔGvdw, ΔGGB, and ΔG_{SA}, were obtained by averaging over the values calculated from the 1000 snapshots extracted from the 10 ns MD trajectories. The parameters used for the MM/GBSA decomposition were same as the energy terms shown in Eqs. 3–5. The only difference is the ΔG_{SA} term, which was estimated based on the SASA with the ICOSA method (Gohlke et al., 2003).

3. Results and discussion

3.1. The dynamic features and binding affinities predicted by MD simulation and MM/GBSA methodology

The root mean square deviations (RMSDs) of the protease backbone were calculated and plotted in Fig. S1 in Supporting Materials, illustrating that almost all of the studied systems are stable along the simulations except ITMN191 with a little shake at 8 ns, but the RMSDs of backbone atoms within 5 Å of ITMN191 undoubtedly confirm that the ITMN191-NS3/4A complex was also stable around the binding pocket (Fig. S2 in Supporting Materials). Subsequently, the root mean square fluctuations (RMSFs) were calculated to explore the dynamic fluctuation of the residues (Fig. S3 in Supporting Materials). The fluctuation patterns of the N-terminus, C-terminus and the loop regions are relatively flexible, while the residues within the active sites (especially the residues 135–139 and 154–160) remain stable, which are consistent with the decomposed binding free energy discussed in the next section that the residues 135–139 and 154–160 bind more favorably with the substrates and inhibitors. Moreover, the average RMSFs for the substrates and inhibitors are 1.508 Å and 1.374 Å, respectively, confirming the higher flexibility of the natural substrates.

The total binding free energies and energetic components are summarized in Table 1. The average binding affinity for the inhibitors is −20.97 kcal/mol, which is −5.67 kcal/mol more favorable than that of the substrates (−15.30 kcal/mol). Therefore, on average, the inhibitors bind more tightly with NS3/4A than the substrates. Besides, the binding affinities of telaprevir, BI201335 and boceprevir (−16.91 kcal/mol, −17.09 kcal/mol and −19.59 kcal/mol, respectively) are obviously weaker than those of TMC435 and ITMN191 (−28.66 kcal/mol and −22.79 kcal/mol). This phenomenon is possibly explained by the ignorance of the covalent bonds between the α-ketoamide groups of telaprevir/boceprevir/BI201335 and the hydroxyl group of Ser139 in the catalytic triad in our simulations (Lin et al., 2006; Perni et al., 2004; Steinkühler et al., 1998). As a result, the predicted binding free energies of the covalent inhibitors were under-estimated by MM/GBSA.

According to the energetic components shown in Table 1, the electrostatic, van der Waals and non-polar desolvation terms are favorable to ligand binding, whereas the polar solvation term and the conformational entropy are unfavorable to ligand binding. The unfavorable polar solvation term (ΔG_{GB}) shows the least correlation with the total binding free energies ($r^2 = 0.28$), and the van der Waals term (ΔE_{vdw}) shows the best linear correlation with the total enthalpies ($r^2 = 0.91$). The electrostatic interactions of the substrates are substantially favorable than those of the inhibitors. However, the favorable electrostatic interactions (ΔE_{elec}) are largely compensated by the unfavorable polar solvation term. When the electrostatic and polar solvation terms are added together, the total polar contributions ($\Delta G_{GB} + \Delta E_{elec}$) also exhibit obvious linear correlation with the total enthalpies ($r^2 = 0.80$). Therefore, both of the polar and non-polar interactions are essential for the binding of the inhibitors and substrates.

3.2. Substrates and inhibitors form similar binding patterns with NS3/4A, whereas the energy distributions of the inhibitors are different from those of the substrates

The binding modes of the natural substrates and inhibitors are shown in Figs. 2 and 3. In order to identify the key residues for ligand binding, we decomposed the total binding free energy into residue-ligand interaction pairs by the MM/GBSA decomposition calculations. The decomposed interaction spectra (Fig. 4) illustrate that the natural substrates and inhibitors form similar binding patterns with three critical regions, including (1) the residues of the catalytic triad (His57, Asp81 and Ser139), (2) the twisted strand 154–160 (Phe154, Arg155, Ala156, Ala157, Val158, Ser159, and Thr160), and (3) the cross-shaped strand 135–139 (Leu135, Lys136, Gly137, Ser138 and Ser139; Ala139 in 4A4B, 4B5A, 5A5B and ITMN191). But the molecular interactions of various ligands are different, and an obvious difference between the inhibitors and substrates is that the substrates form stronger interactions with the cross-shaped strand 135–139 than with the inhibitors, whereas the inhibitors form stronger interactions with the twisted strand 154–160 than the substrates. Specifically, the average contribution percentage of the cross-shaped strand 135–139 for the

Table 1
Binding free energies and energetic components of four inhibitors (ITMN191, boceprevir, TMC435, telaprevir and BI201335) and three natural substrates (4A4B, 4B5A, and 5A5B) of NS3/4A predicted by MM/GBSA (kcal/mol).

Name	ΔE_{vdw}[a]	ΔE_{elec}[b]	ΔG_{GB}[c]	ΔG_{SA}[d]	$-T\Delta S$[e]	$\Delta E_{enthalpy}$[f]	ΔG_{bind}[g]	Average
5A5B	−40.17 ± 0.13[h]	−543.37 ± 1.16	545.87 ± 1.09	−6.55 ± 0.01	28.48 ± 1.34	−44.22 ± 0.17	−15.74 ± 0.17	−15.30
4B5A	−40.22 ± 0.14	−249.48 ± 0.99	252.69 ± 0.87	−6.17 ± 0.01	25.98 ± 0.28	−43.17 ± 0.19	−17.19 ± 0.19	
4A4B	−45.04 ± 0.17	−562.03 ± 1.59	568.52 ± 1.44	−6.89 ± 0.02	32.49 ± 0.68	−45.45 ± 0.23	−12.96 ± 0.23	
ITMN191	−61.32 ± 0.10	−43.92 ± 0.17	59.06 ± 0.14	−7.70 ± 0.01	25.22 ± 0.70	−53.88 ± 0.10	−28.66 ± 0.10	−20.97
TMC435	−61.15 ± 0.14	−28.81 ± 0.19	46.52 ± 0.14	−7.26 ± 0.01	27.92 ± 0.90	−50.71 ± 0.17	−22.79 ± 0.17	
SCH503034	−41.50 ± 0.10	−38.48 ± 0.16	44.12 ± 0.11	−6.27 ± 0.01	25.32 ± 0.54	−42.13 ± 0.11	−16.81 ± 0.11	
VX950	−49.80 ± 0.11	−53.73 ± 0.21	62.43 ± 0.18	−7.15 ± 0.01	28.66 ± 1.32	−48.25 ± 0.12	−19.59 ± 0.12	
BI201335	−63.00 ± 0.11	−46.11 ± 0.19	61.94 ± 0.16	−4.98 ± 0.0.01	35.14 ± 0.10	−52.15 ± 0.11	−17.01 ± 0.11	

[a] van der Waals energy.
[b] Electrostatic energy.
[c] Electrostatic contribution to solvation.
[d] Non-polar contribution to solvation.
[e] Entropic contribution.
[f] Binding free energy in the absence of entropic contribution; [g]binding free energy.
[g] Binding free energy.
[h] Standard deviations based on two blocks (block1: 0–5 ns, block2: 6–10 ns).

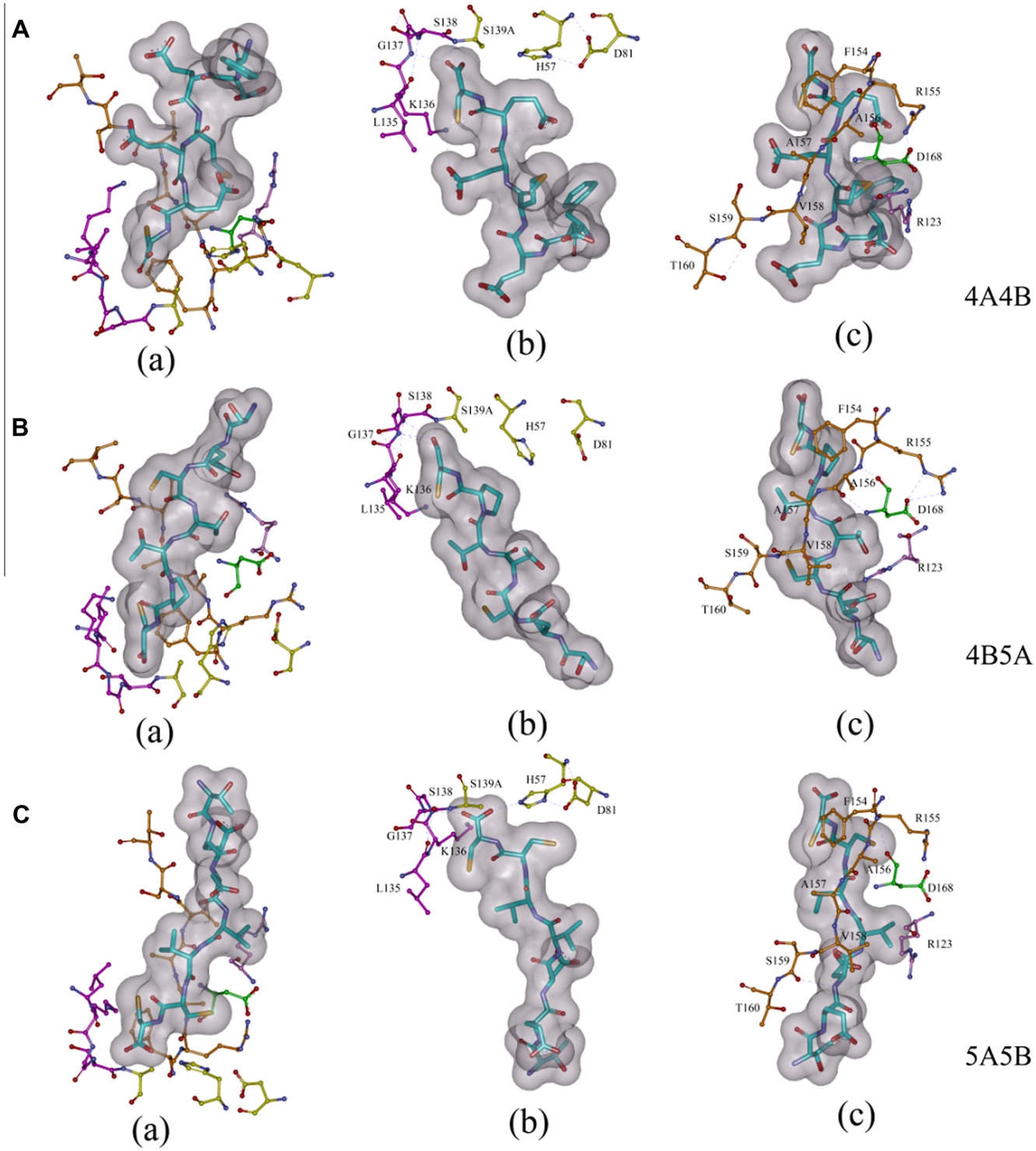

Fig. 2. Dynamic binding modes of the natural substrates (A) 4A4B, (B) 4B5A and (C) 5A5B that bind to (a) the whole three critical regions, (b) the cross-shaped strand 135–139 and the catalytic triad, and (c) the twisted strand 154–160 of NS3/4A, respectively. The substrates are all enclosed in the solvent accessible surfaces; the hydrogen bonds are colored in blue dashed lines; the catalytic triad is marked in yellow, the strand 135–139 in purple, Arg123 in pink, Asp168 in green, and the strand 154–160 in orange. The figures were generated by the Discovery Studio 2.5 molecular simulation package (2009). (For interpretation of the references to color in this figure legend, the reader is referred to the web version of this article.)

substrates (37.08%) is obviously higher than those of the inhibitors (31.40%, 23.34%, 29.81%, 27.095 and 19.21% for ITMN191, boceprevir, TMC435, telaprevir and BI201335, respectively). Meanwhile, the average contribution percentage of the twisted strand 154–160 for the substrates (42.64%) is lower than those of the inhibitors (53.82%, 59.71%, 44.59%, 54.51% and 45.17% for ITMN191, boceprevir, TMC435, telaprevir and BI201335, respectively) (Table 2). That is to say, the natural substrates form balanced interactions with the twisted strand 154–160 and the cross-shaped strand 135–139 (each occupies ~40%), while the inhibitors cannot (the strand 154–160 contributes up to more than 50% of the binding free energy while the strand 135–139 occupies less than 30%). The structural analyses reveal that the strands 135–139 and 154–160 both interact with the P1–P3 moieties of the ligands, but along

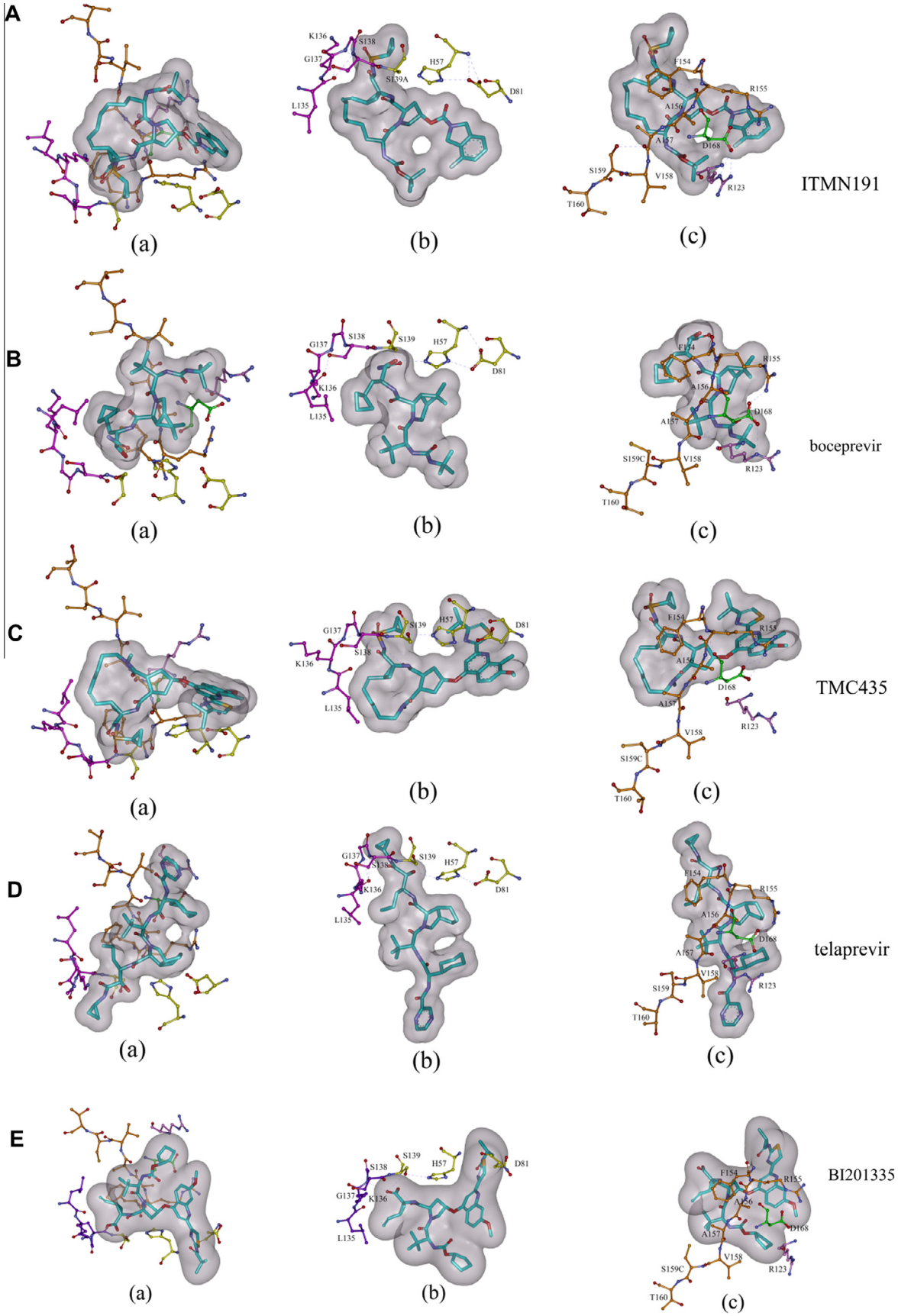

Fig. 3. Dynamic binding modes of the inhibitors (A) ITMN191, (B) boceprevir, (C) TMC435, (D) telaprevir and (E) BI201335 that bind to (a) the whole three critical regions, (b) the cross-shaped strand 135–139 and the catalytic triad, and (c) the twisted strand 154–160 of NS4/4A, respectively. The inhibitors are all enclosed in the solvent accessible surfaces; the hydrogen bonds are colored in blue dashed lines; the catalytic triad is marked in yellow, the strand 135–139 in purple, Arg123 in pink, Asp168 in green, and the strand 154–160 in orange. (For interpretation of the references to color in this figure legend, the reader is referred to the web version of this article.)

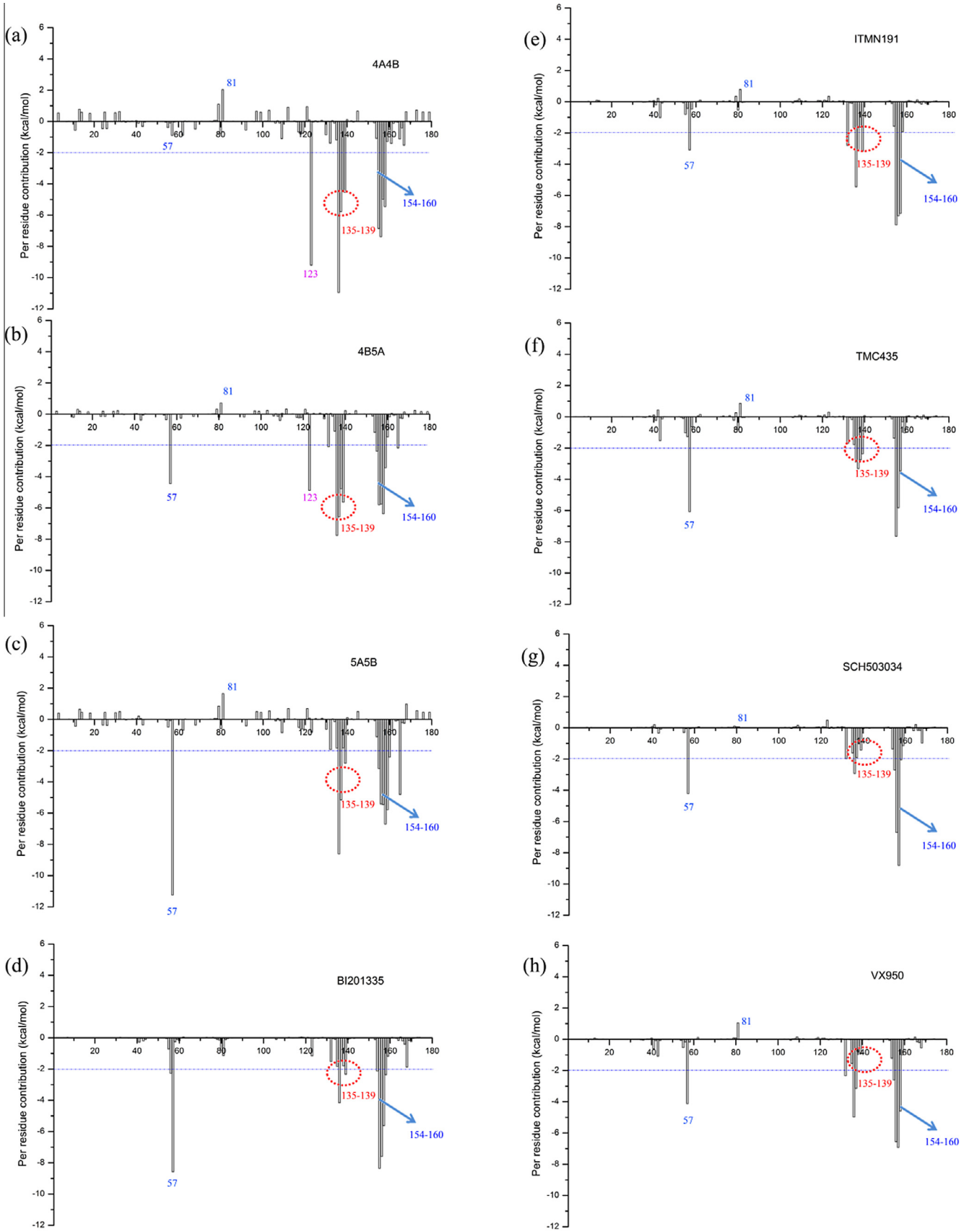

Fig. 4. Binding free energy decomposed spectra for the substrates (a, b, c) and inhibitors (d, e, f, g, h). Critical regions 135–139 are marked in red, and 154–160 in blue. The horizontal ordinate is the residue number. (For interpretation of the references to color in this figure legend, the reader is referred to the web version of this article.)

Table 2
Percentage contributions of three essential zones to the total binding free energies.

	Ave[b]	ITMN191	Boceprevir	TMC435	Telaprevir	BI201335
Triad[a]	12.78%	11.40%	14.64%	17.24%	9.51%	19.97%
135–139	37.08%	31.40%	23.34%	29.81%	27.09%	19.21%
154–160	42.64%	53.82%	59.71%	44.59%	54.51%	45.17%
Total	92.50%	96.62%	97.69%	91.64%	91.11%	84.35%

[a] The catalytic triad region.
[b] Average percentage for the three substrates.

the opposite directions (Figs. 2 and 3). Therefore, the unbalanced distributions can be explained by the competitive interactions between the strands 135–139 and 154–160. When the interactions between the strand 154–160 and an inhibitor become stronger, the corresponding inhibitor will be pulled away from the strand 135–139, thus leading to the decrease of the interactions between the strand 135–139 and this inhibitor, and *vice versa*.

In addition, the contributions of some critical residues to different substrates are also not the same. The substrate 4A4B forms stronger interactions with Lys136 (located at the cross-shaped strand 135–139) than with the substrates 4B5A due to the strong electrostatic interactions of the negatively-charged P5 glutamine acid of 4A4B with Lys136. Arg123 forms favorable van der Waals interaction with 4A4B (−9.202 kcal/mol) but less favorable with 5A5B (−0.820 kcal/mol) owing to the P4 sulfhydryl group of 4A4B. But an interesting finding is that the interaction profiles of the substrates are distinct, however, the overall binding enthalpies for different substrates are conserved at approximately −44 kcal/mol (−44.22 kca/mol, −43.17 kcal/mol, and −45.45 kcal/mol for 5A5B, 4B5A and 4A4B, respectively), suggesting that an optimal and conserved interaction for the diverse substrates is necessary.

3.3. Evaluation of the substrate envelop hypothesis by comparing the interaction profiles of the substrates and inhibitors

By analyzing the crystallographic structures of NS3/4A in complex with substrates or inhibitors, Romano et al. observed that the diverse NS3/4A substrates were recognized in a conserved 3-D shape, thus defining a consensus van der Waals volume or substrate envelope. The mutations conferring severe resistance always occur where the NS3/4A inhibitors protrude from the substrate envelope (Romano et al., 2010, 2011). Initially, the substrate envelope hypothesis was proposed by analyzing the crystallographic structures of the HIV-1 protease-substrate complexes, and it appears that the HIV-1 protease inhibitors that fit within the substrate envelop are less likely to be susceptible to drug-resistant mutations (Özen et al., 2011; Prabu-Jeyabalan et al., 2002). However, any crystallographic structure of NS3/4A only presents a single snapshot trapped in the low energy states of the enzyme (Romano et al., 2010), but the protein–ligand recognition is more closely related to the dynamics of NS3/4A. To remedy the weakness, MD simulations were employed to capture the flexibility of NS3/4A while the free energy calculations and decomposition to characterize the protein–ligand interactions. Here, based on the decomposed interaction spectra, the residue differences between the contributions (G_{res}) were calculated. As shown in Fig. 5, some residues form stronger interactions with the inhibitors than with the substrates. If a value of G_{res} of −1.0 kcal/mol was used as the threshold to predict drug resistance (Hou et al., 2009a), Arg155, Ala156 and Ala157 can confer resistance to ITMN191; Asp81, Ala157 and Asp168 to boceprevir; Phe43, Tyr56, Arg155 to TMC435; Ala157 and Asp168 to telaprevir; and Try56, His57, Asp81, Arg155, Ala156 and Asp168 to BI201335. Encouragingly, among these potential drug resistance sites, the three common mutated sites including Arg155, Ala156, Asp168, are successfully detected. Therefore, the residues involved in drug resistance form stronger interactions with the inhibitors than with the substrates, which are roughly consistent with the conclusions given by the substrate envelope hypothesis (Romano et al., 2010).

Unfortunately, not all mutated sites involved in drug resistance can be correctly predicted by comparing the binding profiles of the inhibitors and substrates. For example, as shown in Table S1, the mutation of Ala156 confers resistance to all drugs. However, according to our predictions, Ala156 forms much stronger interactions with ITMN191 than with the substrates, but forms slightly stronger interactions with boceprevir and telaprevir than with the substrates, even weaker interactions were observed with TMC435 than with the substrates. Therefore, based on our predictions, the mutation of Ala156 is only resistant to ITMN191 and BI201335. Apparently, the predictions from the decomposed energy spectra are not consistent with the experimental data. It is quite possible that a generalized approach or theoretical framework for the prediction of drug resistance is unlikely, and/or that different mutations may confer resistance through different mechanisms. The drug resistance mechanisms for some mutations can only be captured by analyzing the overall residue-interaction network rather than a single residue. For example, the resistance mechanisms of several critical mutated sites might be explained by the perturbation of the electrostatic network. As shown in Table S1 and Fig. 1, the large extended P2′ is closely related to the resistance conferred by the substitution of Asp168. The inhibitors (TMC435, ITMN191, and BI201335) that are trapped in the drug resistance to the mutation of Asp168 always have large extended P2′ fragments, whereas the others (such as telaprevir, boceprevir, and the second generation inhibitor SCH900518) that were dull to the mutation of Asp168, do not have such large extended P2′ fragments. Moreover, the newly-developed inhibitor, ACH1625, which is resistant to the mutation of Asp168, also contains a large P2′ (Huang et al., 2010). According to Fig. 4 and Table S4, Asp168 does not form strong interactions with any substrate or inhibitor (Fig. 4). Nevertheless, Asp168 builds a large electrostatic network with Arg155, Arg123, Ala156 and Asp81 (Figs. 2 and 3). In this network, Arg155 and Ala156 interact strongly with ITMN191, TMC435 and BI201335 by stacking with the large extended P2′ fragments. And we suppose that the essential function of Asp168 is to stabilize the conformation of Arg155 to maintain the favorable interaction between Arg155 and the P2′ fragments of ligands. Therefore, the mutation of Asp168 may destroy the salt bridges with Arg123 and Arg155, and then impairs the conformational stability of Arg155 and destroys its binding with ligands, especially those inhibitors with the large P2′ fragments, for instance ITMN191,TMC435 and BI201335. On the contrary, for the substrates and linear inhibitors without large extended P2′ fragments, such as boceprevir and telaprevir, their interactions with Arg155 (−2.71 kcal/mol and −2.61 kcal/mol) are weaker than those with TMC435, ITMN191 and BI201335 (−7.65 kcal/mol, −7.89 kcal/mol and −8.36 kcal/mol, respectively), and therefore, the mutation of Asp168 does not have large impact on their binding with NS3/4A.

3.4. Recovering the unbalanced interactions between inhibitor and protein may be an effective way to combat drug resistance

The analysis in Section 3.2 illustrates the substrates could gain balanced interactions with the strands 135–139 and 154–160, but the studied inhibitors cannot. Therefore, it is quite possible that the unbalanced interactions are related to the NS3/4A drug resistance to the current inhibitors. The following reasons may lead to the unbalanced energy distributions: (1) first, the energy contribution of the residues 135–139 to the substrates is higher than that to the inhibitors (Fig. 4). The exist of electrostatic network between the

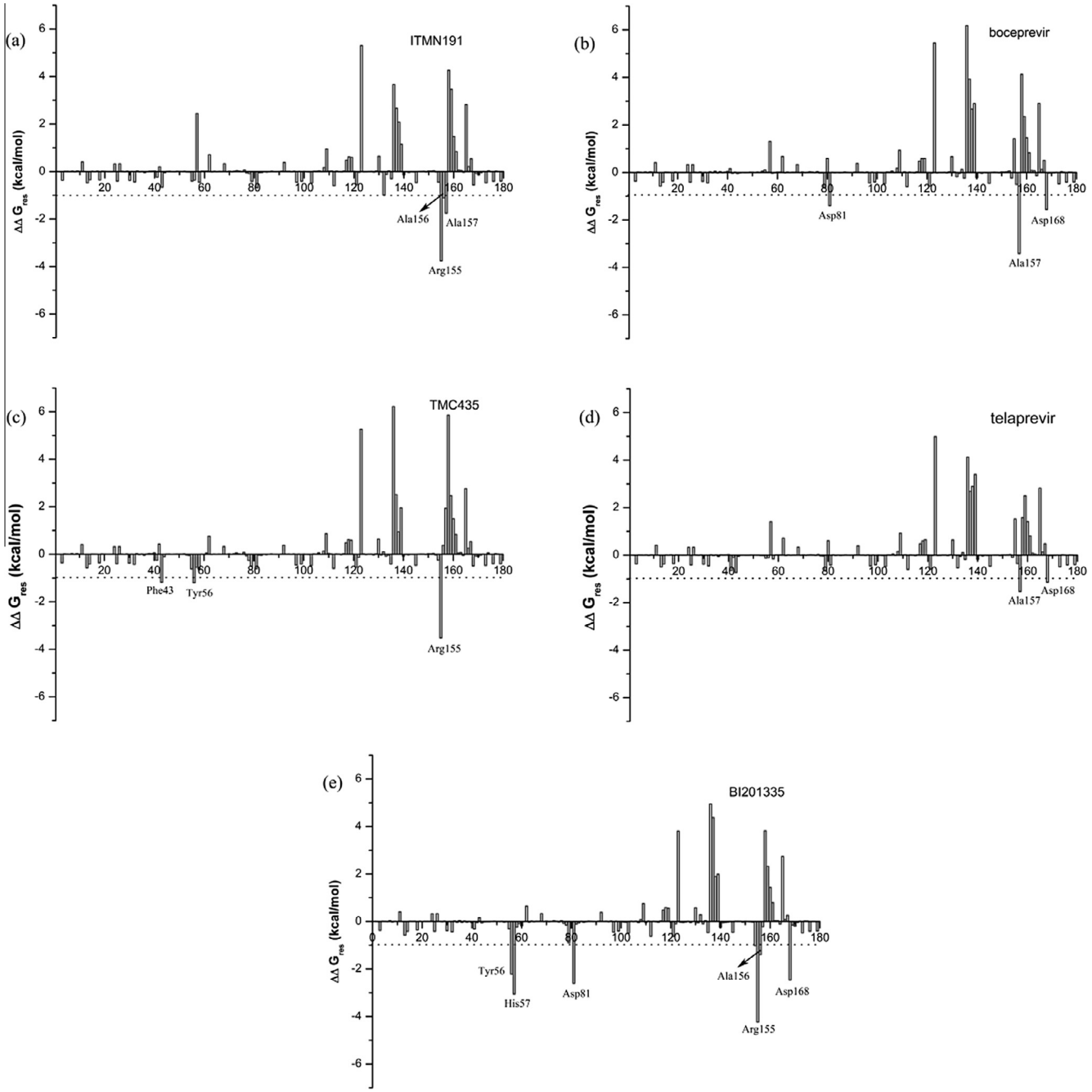

Fig. 5. Difference between the contributions of each protease residue to the binding free energy of (a) ITMN191, (b) boceprevir, (c) TMC435, (d) telaprevir or (e) BI201335 and the substrates ($\Delta\Delta G_{res}$). $\Delta\Delta G_{res} = \Delta G_{bind}^{inhibitor} - \Delta G_{bind}^{ave}$ and the ΔG_{bind}^{ave} is the average free energy of the three substrates.

strand 135–139 and the P1–P2 fragments of the substrates, may partly explain the difference. The binding pattern of the substrate 4B5A was analyzed as an example: the carbonyl acid of P1 forms four H-bonds with the residues Gly137, Ser138 and Ala139 and then contacts with Leu135 to form an electrostatic network (Fig. 2B), however, no such electrostatic network exists for the inhibitors. Even the inhibitor BI201335 also has a similar free carbonyl acid at the P1 site, but its terminal oxygen of P1 forms intramolecular H-bond with the P2 carbonyl, which restraints the formation of the electrostatic network. In addition, Lys136 is of only −4.06 kcal/mol binding free energy to the inhibitors, but ∼−9.11 kcal/mol to the substrates. The modeling analysis illustrates that that the long side-chain of Lys136 spans from P1 to P3 of the substrates and its terminal amide nitrogen forms H-bonds with the carbonyl oxygen of P2–P3 of the substrates, but such interactions are not observed for the inhibitors. Therefore, the electrostatic interactions between the strand 135 and 139 and the substrates are stronger than those between the strand 135 and 139 and the inhibitors. (2) The binding patterns of Val158 and Ser159 with the inhibitors and substrates are different. Val158 and Ser159 contact with the P6–P7 fragments of the substrates and form favorable interactions with them (−6.18 kcal/mol and −3.50 kcal/mol). However, the interactions of the inhibitors with Val158 and Ser159 (−2.22 kcal/mol and −0.81 kcal/mol) are much weaker due to the fact that the P6–P7 moieties of the NS3/4A inhibitors are truncated. Nonetheless, the inhibitors without the P6–P7 moieties form stronger binding affinities with the strand 154–160 than the substrates (Table 2) due to some extraordinary contributions. Apparently, among the residues 154–160, Arg155 forms more favorable interaction with TMC435,

ITMN191 and BI201335 (−7.65 kcal/mol, −7.89 kcal/mol and −8.36 kcal/mol, respectively) due to the stronger van der Waals interactions with the large extended P2′ fragment, but ITMN191, telaprevir, boceprevir and BI201335 form stronger interactions with Ala156 (−7.31 kcal/mol, −6.56 kcal/mol, −6.71 kcal/mol and −7.60 kcal/mol, respectively) and Ala157 (−7.15 kcal/mol, −6.93 kcal/mol, −8.82 kcal/mol and −5.62 kcal/mol, respectively). Therefore, the total binding affinities of the inhibitors with the strand 154–160 are stronger than those of the substrates. In conclusion, the weaker interaction with the strand 135–139 while stronger interactions with the strand 154–160 lead to the unbalanced interaction distributions for the inhibitors.

In summary, we predict that the unbalanced interactions between the strands 135–139 and 154–160 are closely related to the drug resistance. So in order to develop novel candidates to overcome the drug resistance, it might be necessary to regain the balanced interactions between the two strands. Specifically, modifications should focus on enhancing the interactions with the strand 135–139 while attenuating the interactions with the strand 154–160. First, the inhibitors that are easily trapped into drug resistance dilemma always have a large P2′ fragment, and thus easily lost the balance with the strands 135–139 and 154–160. Therefore, appropriately attenuating the interactions between the strand 154–160 and the P2′ fragments of an inhibitor may be helpful to regain the balance, specifically, decreasing the size of the P2′ fragment of an inhibitor by trimming or substituting the aromatic rings at P2′ to lower the van der Waals interaction with Arg155. Subsequently, to compensate the energy loss of the strand 154–160, the interactions between the strand 135–139 and P1–P1′ should be enhanced. Since the carbonyl oxygen at P1 is essential to form the H-bonds with the amide nitrogen of NS3/4A, it may be helpful to introduce some acidic carbonyl group or others into the P1 segment of an inhibitor. Second, the interaction between Lys136 and the P2–P3 fragments of inhibitors can be enhanced by introducing H-bond receptor groups or some functional groups such as acidic carbonyl or sulfonic acid that can form electrostatic interactions with the alkalic amino of Lys136. Certainly, these modifications may affect the biological properties of the inhibitor, especially the ADMET (absorption, distribution, metabolism, excretion and toxicity) properties, so a good balance between satisfactory capability to combat drug resistance and favorable ADMET properties should be considered.

4. Conclusion

In this study, MD simulations and MM/GBSA free energy calculation were employed to characterize the energetic interaction patterns of NS3/4A bound with the inhibitors or substrates. The residue-ligand interaction spectra illustrate that the studied inhibitors and substrates share similar binding patterns, and they can form strong interactions with the catalytic triad, the cross-shaped strand 135–139 and the twist strand 154–160. The residue-ligand interaction profiles of five inhibitors and three natural substrates of NS3/4A were compared, and the results obtained partially support the general molecular basis of drug resistance: the critical resistant mutations impair more to the binding of the inhibitors than that of the substrates, which is roughly consistent with the predictions from the substrate envelope hypothesis. Different from the substrate envelope hypothesis derived from the analysis of crystallographic data, the comparison of the dynamic residue-ligand interaction profiles between the substrates and inhibitors provides a more accurate and quantitative way to capture the competitive binding between the inhibitors and substrates of NS3/4A. It should be pointed out that different mutations may confer resistance through different mechanisms and a generalized approach or theoretical framework for the prediction of drug resistance may not exist. The drug resistant mechanism can only be captured by analyzing the overall residue-interaction network rather than a single residue. In addition, the calculation results illustrate that the balanced interaction with the twisted strand 154–160 and the cross-shaped strand 135–139 might be essential to achieve good capability in combating drug resistance.

Acknowledgements

This study was supported by the National Science Foundation of China (21173156), the National Basic Research Program of China (973 program, 2012CB932600), Specialized Research Fund for the Doctoral Program of Higher Education (20123201110017), and the Priority Academic Program Development of Jiangsu Higher Education Institutions (PAPD).

Appendix A. Supplementary data

Supplementary data associated with this article can be found, in the online version, at http://dx.doi.org/10.1016/j.antiviral.2014.01.010.

References

Discovery Studio 2.5 Guide, Accelrys Inc., San Diego, 2009, http://www.accelrys.com.
Almasio, P.L., Cottone, C., D'Angelo, F., 2007. Pegylated interferon therapy in chronic hepatitis C: lights and shadows of an innovative treatment. Dig. Liver Dis. 39, S88–S95.
Bacon, B.R., Gordon, S.C., Lawitz, E., Marcellin, P., Vierling, J.M., Zeuzem, S., Poordad, F., Goodman, Z.D., Sings, H.L., Boparai, N., 2011. Boceprevir for previously treated chronic HCV genotype 1 infection. N. Engl. J. Med. 364, 1207–1217.
Bayly, C.I., Cieplak, P., Cornell, W., Kollman, P.A., 1993. A well-behaved electrostatic potential based method using charge restraints for deriving atomic charges: the RESP model. J. Phys. Chem. 97, 10269–10280.
Brooks, B., Karplus, M., 1983. Harmonic dynamics of proteins: normal modes and fluctuations in bovine pancreatic trypsin inhibitor. Proc. Natl. Acad. Sci. U.S.A. 80, 6571–6575.
Case, D.A., Cheatham, T.E., Darden, T., Gohlke, H., Luo, R., Merz, K.M., Onufriev, A., Simmerling, C., Wang, B., Woods, R.J., 2005. The Amber biomolecular simulation programs. J. Comput. Chem. 26, 1668–1688.
Colson, P., Brouk, N., Lembo, F., Castellani, P., Tamalet, C., Gerolami, R., 2008. Natural presence of substitution R155K within hepatitis C virus NS3 protease from a treatment-naïve chronically infected patient. Hepatology 47, 766–767.
Darden, T., York, D., Pedersen, L., 1993. Particle mesh Ewald: an N log (N) method for Ewald sums in large systems. J. Chem. Phys. 98, 10089.
Forestier, N., Larrey, D., Marcellin, P., Guyader, D., Patat, A., Rouzier, R., Smith, P.F., Qin, X., Lim, S., Bradford, W., 2011. Antiviral activity of danoprevir (ITMN-191/RG7227) in combination with pegylated interferon α-2a and ribavirin in patients with hepatitis C. J. Infect. Dis. 204, 601–608.
Fried, M.W., Shiffman, M.L., Reddy, K.R., Smith, C., Marinos, G., Gonçales Jr, F.L., Häussinger, D., Diago, M., Carosi, G., Dhumeaux, D., 2002. Peginterferon alfa-2a plus ribavirin for chronic hepatitis C virus infection. N. Engl. J. Med. 347, 975–982.
Frisch, M.J., Trucks, G., Schlegel, H., Scuseria, G., Robb, M., Cheeseman, J., Scalmani, G., Barone, V., Mennucci, B., Petersson, G., 2009. Gaussian 09. Gaussian. Inc., Wallingford, CT.
Gohlke, H., Kiel, C., Case, D.A., 2003. Insights into protein-protein binding by binding free energy calculation and free energy decomposition for the Ras-Raf and Ras-RalGDS complexes. J. Mol. Biol. 330, 891–913.
Halfon, P., Locarnini, S., 2011. Hepatitis C virus resistance to protease inhibitors. J. Hepatol. 55, 192–206.
Hornak, V., Abel, R., Okur, A., Strockbine, B., Roitberg, A., Simmerling, C., 2006. Comparison of multiple Amber force fields and development of improved protein backbone parameters. Proteins: Struct. Funct. Bioinf. 65, 712–725.
Hou, T., Zhang, W., Wang, J., Wang, W., 2009a. Predicting drug resistance of the HIV-1 protease using molecular interaction energy components. Proteins: Struct. Funct. Bioinf. 74, 837–846.
Hou, T.J., Li, N., Li, Y., Wang, W., 2012. Characterization of domain-peptide interaction interface. Prediction of SH3 domain-mediated protein-protein interaction network in yeast by generic structure-based models. J. Proteome Res. 11, 2982–2995.
Hou, T.J., McLaughlin, W.A., Wang, W., 2008a. Evaluating the potency of HIV-1 protease drugs to combat resistance. Proteins: Struct. Funct. Bioinf. 71, 1163–1174.
Hou, T.J., Wang, J., Li, Y.Y., Wang, W., 2011a. Assessing the performance of the MM/PBSA and MM/GBSA methods: I. The accuracy of binding free energy

calculations based on molecular dynamics simulations. J. Chem. Inf. Model. 51, 69–82.
Hou, T.J., Wang, J., Li, Y.Y., Wang, W., 2011b. Assessing the performance of the molecular mechanics/Poisson Boltzmann surface area and molecular mechanics/generalized born surface area methods. II. The accuracy of ranking poses generated from docking. J. Comput. Chem. 32, 866–877.
Hou, T.J., Xu, Z., Zhang, W., McLaughlin, W.A., Case, D.A., Xu, Y., Wang, W., 2009b. Characterization of domain-peptide interaction interface. A generic structure-based model to decipher the binding specificity of SH3 domains. Mol. Cell. Proteomics 8, 639–649.
Hou, T.J., Yu, R., 2007. Molecular dynamics and free energy studies on the wild-type and double mutant HIV-1 protease complexed with amprenavir and two amprenavir-related inhibitors: mechanism for binding and drug resistance. J. Med. Chem. 50, 1177–1188.
Hou, T.J., Zhang, W., Case, D.A., Wang, W., 2008b. Characterization of domain-peptide interaction interface. A case study on the amphiphysin-1 SH3 domain. J. Mol. Biol. 376, 1201–1214.
Huang, M., Fabrycki, J., Patel, D., Podos, S., Yang, G., Zhao, Y., Marlor, C., Stauber, K., Agarwal, A., Wang, X., 2010. 650 antiviral activity, combination and resistance of ACH-1625, a potent, clinical stage HCV NS3 protease inhibitor. J. Hepatol. 52, S254.
Huo, S., Wang, J., Cieplak, P., Kollman, P.A., Kuntz, I.D., 2002. Molecular dynamics and free energy analyses of cathepsin D-inhibitor interactions: insight into structure-based ligand design. J. Med. Chem. 45, 1412–1419.
Jamall, I.S., Yusuf, S., Azhar, M., Jamall, S., 2008. Is pegylated interferon superior to interferon, with ribavarin, in chronic hepatitis C genotypes 2/3? World J. gastroenterol. 14, 6627.
Jorgensen, W.L., Chandrasekhar, J., Madura, J.D., Impey, R.W., Klein, M.L., 1983. Comparison of simple potential functions for simulating liquid water. J. Chem. Phys. 79, 926.
Karthick, V., Shanthi, V., Rajasekaran, R., Ramanathan, K., 2012. Exploring the cause of oseltamivir resistance against mutant H274Y neuraminidase by molecular simulation approach. J. Phys. Chem. B., 1–13.
Kollman, P.A., Massova, I., Reyes, C., Kuhn, B., Huo, S., Chong, L., Lee, M., Lee, T., Duan, Y., Wang, W., 2000. Calculating structures and free energies of complex molecules: combining molecular mechanics and continuum models. Acc. Chem. Res. 33, 889–897.
Lemke, C.T., Goudreau, N., Zhao, S., Hucke, O., Thibeault, D., Llinàs-Brunet, M., White, P.W., 2011. Combined X-ray, NMR, and kinetic analyses reveal uncommon binding characteristics of the hepatitis C virus NS3–NS4A protease inhibitor BI 201335. J. Biol. Chem. 286, 11434–11443.
Lenz, O., Verbinnen, T., Lin, T.-I., Vijgen, L., Cummings, M.D., Lindberg, J., Berke, J.M., Dehertogh, P., Fransen, E., Scholliers, A., 2010. In vitro resistance profile of the hepatitis C virus NS3/4A protease inhibitor TMC435. Antimicrob. Agents Chemother. 54, 1878–1887.
Li, L., Li, Y.Y., Zhang, L.L., Hou, T.J., 2012. Theoretical studies on the susceptibility of oseltamivir against variants of 2009 A/H1N1 influenza neuraminidase. J. Chem. Inf. Model. 52, 2715–2729.
Li, M.S., Nguyen, T.T., Mai, B.K., 2011. Study of Tamiflu Sensitivity to Variants of A/H5N1 Virus Using Different Force Fields. J. Chem. Inf. Model..
Lin, C., Kwong, A., Perni, R., 2006. Discovery and development of VX-950, a novel, covalent, and reversible inhibitor of hepatitis c virus NS3* 4A serine protease. Infect. Disord. Drug Targets 6.
Liu, H., Yao, X., Wang, C., Han, J., 2010. In silico identification of the potential drug resistance sites over 2009 influenza A (H1N1) virus neuraminidase. Mol. Pharm. 7, 894–904.
Malcolm, B., Liu, R., Lahser, F., Agrawal, S., Belanger, B., Butkiewicz, N., Chase, R., Gheyas, F., Hart, A., Hesk, D., 2006. SCH 503034, a mechanism-based inhibitor of hepatitis C virus NS3 protease, suppresses polyprotein maturation and enhances the antiviral activity of alpha interferon in replicon cells. Antimicrob. Agents Chemother. 50, 1013–1020.
Manabe, S., Fuke, I., Tanishita, O., Kaji, C., Gomi, Y., Yoshida, S., Mori, C., Takamizawa, A., Yosida, I., Okayama, H., 1994. Production of nonstructural proteins of hepatitis C virus requires a putative viral protease encoded by NS3. Virology 198, 636–644.
McHutchison, J.G., Everson, G.T., Gordon, S.C., Jacobson, I.M., Sulkowski, M., Kauffman, R., McNair, L., Alam, J., Muir, A.J., 2009. Telaprevir with peginterferon and ribavirin for chronic HCV genotype 1 infection. N. Engl. J. Med. 360, 1827–1838.
McHutchison, J.G., Manns, M.P., Muir, A.J., Terrault, N.A., Jacobson, I.M., Afdhal, N.H., Heathcote, E.J., Zeuzem, S., Reesink, H.W., Garg, J., 2010. Telaprevir for previously treated chronic HCV infection. N. Engl. J. Med. 362, 1292–1303.
Miller III, B.R., McGee, T.D., Swails, J.M., Homeyer, N., Gohlke, H., Roitberg, A.E., 2012. MMPBSA. py: An efficient program for end-state free energy calculations. J. Chem. Theory. Comput., 3314–3321.
Moradpour, D., Penin, F., Rice, C.M., 2007. Replication of hepatitis C virus. Nat. Rev. Microbiol. 5, 453–463.
Onufriev, A., Bashford, D., Case, D.A., 2004. Exploring protein native states and large-scale conformational changes with a modified generalized born model. Proteins: Struct. Funct. Bioinf. 55, 383–394.
Ozen, A., Haliloglu, T., Schiffer, C.A., 2011. Dynamics of preferential substrate recognition in HIV-1 protease: redefining the substrate envelope. J. Mol. Biol. 410, 726–744.
Özen, A., Haliloğlu, T., Schiffer, C.A., 2011. Dynamics of preferential substrate recognition in HIV-1 protease: redefining the substrate envelope. J. Mol. Biol. 410, 726–744.
Pan, D., Xue, W., Zhang, W., Liu, H., Yao, X., 2012. Understanding the drug resistance mechanism of hepatitis C virus NS3/4A to ITMN-191 due to R155K, A156V, D168A/E mutations: a computational study. Biochim. Biophys. Acta (BBA)-Gen. Subj. 1820, 1526–1534.
Perni, R.B., Almquist, S.J., Byrn, R.A., Chandorkar, G., Chaturvedi, P.R., Courtney, L.F., Decker, C.J., Dinehart, K., Gates, C.A., Harbeson, S.L., 2006. Preclinical profile of VX-950, a potent, selective, and orally bioavailable inhibitor of hepatitis C virus NS3-4A serine protease. Antimicrob. Agents Chemother. 50, 899–909.
Perni, R.B., Pitlik, J., Britt, S.D., Courtney, L.F., Deininger, D.D., Farmer, L.J., Gates, C.A., Harbeson, S.L., Levin, R.B., Lin, C., 2004. Inhibitors of hepatitis C virus NS3 4A protease 2. Warhead SAR and optimization. Bioorg. Med. Chem. Lett. 14, 1441–1446.
Prabu-Jeyabalan, M., Nalivaika, E., Schiffer, C.A., 2002. Substrate shape determines specificity of recognition for HIV-1 protease: analysis of crystal structures of six substrate complexes. Structure 10, 369–381.
Romano, K.P., Ali, A., Aydin, C., Soumana, D., Özen, A., Deveau, L.M., Silver, C., Cao, H., Newton, A., Petropoulos, C.J., 2012. The molecular basis of drug resistance against hepatitis C virus NS3/4A protease inhibitors. PLoS Pathog. 8, e1002832.
Romano, K.P., Ali, A., Royer, W.E., Schiffer, C.A., 2010. Drug resistance against HCV NS3/4A inhibitors is defined by the balance of substrate recognition versus inhibitor binding. Proc. Natl. Acad. Sci. U.S.A. 107, 20986–20991.
Romano, K.P., Laine, J.M., Deveau, L.M., Cao, H., Massi, F., Schiffer, C.A., 2011. Molecular mechanisms of viral and host cell substrate recognition by hepatitis C virus NS3/4A protease. J. Virol. 85, 6106–6116.
Rong, L., Dahari, H., Ribeiro, R.M., Perelson, A.S., 2010. Rapid emergence of protease inhibitor resistance in hepatitis C virus. Sci. Transl. Med. 2, 30ra32.
Ryckaert, J.-P., Ciccotti, G., Berendsen, H.J., 1977. Numerical integration of the cartesian equations of motion of a system with constraints: molecular dynamics of n-alkanes. J. Comput. Phys. 23, 327–341.
Sarrazin, C., Zeuzem, S., 2010. Resistance to direct antiviral agents in patients with hepatitis C virus infection. Gastroenterology 138, 447–462.
Shimakami, T., Welsch, C., Yamane, D., McGivern, D.R., Yi, M., Zeuzem, S., Lemon, S.M., 2011. Protease inhibitor-resistant hepatitis C virus mutants with reduced fitness from impaired production of infectious virus. Gastroenterology 140, 667–675.
Steinkühler, C., Biasiol, G., Brunetti, M., Urbani, A., Koch, U., Cortese, R., Pessi, A., De Francesco, R., 1998. Product inhibition of the hepatitis C virus NS3 protease. Biochemistry 37, 8899–8905.
Sun, H.Y., Ji, F.Q., 2012. A molecular dynamics investigation on the crizotinib resistance mechanism of C1156Y mutation in ALK. Biochem. Biophys. Res. Commun. 423, 319–324.
Tong, X., Arasappan, A., Bennett, F., Chase, R., Feld, B., Guo, Z., Hart, A., Madison, V., Malcolm, B., Pichardo, J., 2010. Preclinical characterization of the antiviral activity of SCH 900518 (narlaprevir), a novel mechanism-based inhibitor of hepatitis C virus NS3 protease. Antimicrob. Agents Chemother. 54, 2365–2370.
Wang, J., Wolf, R.M., Caldwell, J.W., Kollman, P.A., Case, D.A., 2004. Development and testing of a general amber force field. J. Comput. Chem. 25, 1157–1174.
Wang, J.M., Hou, T.J., Xu, X.J., 2006. Recent advances in free energy calculations with a combination of molecular mechanics and continuum models. Curr. Comput.-Aided Drug Des. 2, 287–306.
Wang, W., Kollman, P.A., 2001. Computational study of protein specificity: the molecular basis of HIV-1 protease drug resistance. Proc. Natl. Acad. Sci. U.S.A. 98, 14937–14942.
Weiser, J., Shenkin, P.S., Still, W.C., 1999. Approximate atomic surfaces from linear combinations of pairwise overlaps (LCPO). J. Comput. Chem. 20, 217–230.
Welsch, C., Jesudian, A., Zeuzem, S., Jacobson, I., 2012a. New direct-acting antiviral agents for the treatment of hepatitis C virus infection and perspectives. Gut 61, i36–i46.
Welsch, C., Schweizer, S., Shimakami, T., Domingues, F.S., Kim, S., Lemon, S.M., Antes, I., 2012b. Ketoamide resistance and hepatitis C virus fitness in Val55 variants of the NS3 serine protease. Antimicrob. Agents Chemother. 56, 1907–1915.
Wohnsland, A., Hofmann, W.P., Sarrazin, C., 2007. Viral determinants of resistance to treatment in patients with hepatitis C. Clin. Microbiol. Rev. 20, 23–38.
Xu, L., Sun, H., Li, Y., Wang, J., Hou, T., 2013. Assessing the performance of MM/PBSA and MM/GBSA methods. 3. The impact of force fields and ligand charge models. J. Phys. Chem. B 117, 8408–8421.
Xue, W., Pan, D., Yang, Y., Liu, H., Yao, X., 2012a. Molecular modeling study on the resistance mechanism of HCV NS3/4A serine protease mutants R155K, A156V and D168A to TMC435. Antivir. Res. 93, 126–137.
Xue, W., Wang, M., Jin, X., Liu, H., Yao, X., 2012b. Understanding the structural and energetic basis of inhibitor and substrate bound to the full-length NS3/4A: insights from molecular dynamics simulation, binding free energy calculation and network analysis. Mol. Biosyst. 8, 2753–2765.
Xue, W.W., Qi, J., Yang, Y., Jin, X.J., Liu, H.X., Yao, X.J., 2012c. Understanding the effect of drug-resistant mutations of HIV-1 intasome on raltegravir action through molecular modeling study. Mol. BioSyst. 8, 2135–2144.
Yang, Y., Liu, H., Yao, X., 2012. Understanding the molecular basis of MK2–p38α signaling complex assembly: insights into protein–protein interaction by molecular dynamics and free energy studies. Mol. Biosyst. 8, 2106–2118.
Yang, Y., Qin, J., Liu, H., Yao, X., 2011a. Molecular dynamics simulation, free energy calculation and structure-based 3D-QSAR studies of B-RAF kinase inhibitors. J. Chem. Inf. Model. 51, 680–692.
Yang, Y., Shen, Y., Liu, H., Yao, X., 2011b. Molecular dynamics simulation and free energy calculation studies of the binding mechanism of allosteric inhibitors with p38α MAP kinase. J. Chem. Inf. Model. 51, 3235–3246.
Zhang, J., Hou, T., Wang, W., Liu, J.S., 2010. Detecting and understanding combinatorial mutation patterns responsible for HIV drug resistance. Proc. Natl. Acad. Sci. U.S.A. 107, 1321–1326.